Direct comparison of optimized effective potential and Hartree-Fock self-consistent calculations for jellium slabs

H. Luo,[1] C. M. Horowitz,[2] H.-J. Flad,[3] C. R. Proetto,[4] and W. Hackbusch[1]

[1]*Max-Planck-Institut für Mathematik in den Naturwissenschaften, Inselstrasse 22-26, D-04103 Leipzig, Germany*

[2]*Instituto de Investigaciones Fisicoquímicas Teóricas y Aplicadas (INIFTA), UNLP, CCT La Plata-CONICET, Sucursal 4, Casilla de Correo 16, La Plata, Argentina*

[3]*Institut für Mathematik, Technische Universität Berlin, Straße des 17, Juni 137, D-10623 Berlin, Germany*

[4]*Centro Atómico Bariloche and Instituto Balseiro, 8400 San Carlos de Bariloche, Río Negro, Argentina*

(Received 4 August 2011; revised manuscript received 19 March 2012; published 20 April 2012)

We present a direct comparison of the exchange-only optimized effective potential (x-OEP) method, originating from density functional theory, with Hartree-Fock (HF) results for jellium slabs of finite width, based on fully self-consistent calculations. The nonlocal character of the HF exchange potential causes a coupling of the momentum parallel to the slab surface with the perpendicular component of the orbitals. This results in an entirely different energy-band structure close to the Fermi surface and in terms of bandwidth, as compared with the x-OEP energy-band structure. Good agreement between x-OEP and HF calculations for jellium slabs has been observed for Friedel oscillations of the electron density, surface energies, and dipole barriers, as well as for electrostatic and averaged exchange potentials. However, marked differences appear between x-OEP and HF work functions for narrow slabs, which is in contrast to the good agreement of ionization energies reported for finite systems. On the other hand, we present evidence that both work functions are very similar in the limit of very wide slabs.

DOI: 10.1103/PhysRevB.85.165133 PACS number(s): 71.10.Ca, 73.20.At, 31.15.E−

I. INTRODUCTION

The antisymmetry of fermionic wave functions, which is a consequence of Pauli's exclusion principle, determines to a large extent the properties of electronic systems. At the basic level of the *Hartree-Fock* (HF) approximation, the exclusion principle is rigorously satisfied by the ansatz for a many-electron wave function via a single Slater determinant and expresses itself in the HF equation via the nonlocal exchange term.[1] Because of its computational complexity, various local approximations of exchange contributions have been suggested for the HF formalism; cf. Ref. 2 and references therein. The most prominent variant is Slater's X-α model[3] that transfers the exchange from the homogeneous electron gas by a local approximation to atoms, molecules, and solids. With the emergence of *density functional theory* (DFT), these approximate HF treatments became obsolete, but Slater's local exchange remained, with a minor modification regarding the prefactor (a constant), as the leading-order term in almost every approximation to the "exact" but unknown Kohn-Sham exchange-correlation potential; cf. Ref. 4 for further details. The most disturbing feature of Slater's local exchange is the spurious self-interaction energy of electrons due to an inexact cancellation between the Hartree and approximate (local) exchange potential.[5] Further developments in DFT such as work by Becke,[6,7] within the framework of generalized gradient corrections,[8,9] only partially resolved this problem; cf. Ref. 10. An alternative scheme, already suggested by Kohn and Sham,[11] takes a nonlocal exchange potential as a preassigned part of the *Kohn-Sham* (KS) equation and leaves only an unknown correlation potential to be determined. This ansatz became known as the *Hartree-Fock-Kohn-Sham* (HFKS) method; cf. Ref. 4 for further details. A mixture of exact (single-determinant) and local exchange in the energy functional, with an adjustable mixing parameter, has also been considered by Becke.[12] While these so-called hybrid functionals perform significantly better than purely local functionals, they have, however, a conceptual shortcoming due to the use of a nonlocal exchange potential.[13] In order to stay in the original DFT framework of the KS equation, it is, however, possible to consider the exact (single-determinant) exchange energy functional E_x as an implicit functional of the electron density, but as an explicit functional of the KS orbitals, and to rigorously derive a corresponding local exchange potential.[14,15] This procedure can be seen in the more general framework of the *optimized effective potential* (OEP) method,[16,17] which allows one to incorporate orbital-dependent exchange-correlation energy functionals into the DFT formalism. Its simplest variant is the exchange-only (x-OEP) approximation, where correlation is completely neglected; one can consider the resulting KS equation as a local approximation of the HF equation. This has to be understood in the sense that the x-OEP potential represents the local exchange potential for which the solutions of the KS equation give the lowest energy. The x-OEP method requires the simultaneous solution of the KS equation and an additional integral equation for the calculation of the local exchange potential. This rather demanding computational scheme can be simplified, however, by an accurate approximation of the integral equation suggested by Krieger *et al.* (KLI).[18] Typically, HF and x-OEP ground-state energies are very close; however, they are not the same.[19–21] The reason is simple:[20,22] in both cases, a variational optimization of the *same* exchange energy functional is performed. In the HF method, the optimization is performed with respect to the orbitals, while in the x-OEP method, the optimization is performed with respect to the exchange potential, which is requested to be local. Since in the x-OEP method an extra

constraint is then fulfilled, the variational ground-state HF energy is always lower than the one resulting from the x-OEP constrained optimization. As we show below, this important distinction between HF and x-OEP ground-state energies is strictly satisfied in our self-consistent calculations for metallic jellium slabs. Comparative numerical studies of HF and x-OEP calculations for atoms, molecules, and solids have been reported in the literature and have demonstrated good agreement for a large variety of properties.[16,22,23] Here, we want to include in this list our metallic jellium slab system, and explore whether a careful, thorough numerical study of such a paradigmatic system may reveal those quantities, if any, which differ significantly between HF and x-OEP.

For the case of extended (periodic) systems, a serious shortcoming of the HF electronic band structure has been already proved.[24] On rather general grounds, it was found that the HF density of states (DOS) of real metallic systems beyond the homogeneous electron gas displays an improper singularity at the Fermi energy. This leads to a vanishing of the DOS at the Fermi surface, regardless of the Fermi-surface shape. The result applies to extended (periodic) systems in three dimensions (3D), 2D, and 1D. As we will show below, it also applies to our slab metallic system, which is finite (nonperiodic) in the slab coordinate, but is infinite in the perpendicular (in-plane) directions.

In our previous work, we separately studied jellium slabs within the x-OEP[25,26] and HF[27] approximations. Now, we present a detailed HF versus x-OEP study for jellium slabs, which represents an important benchmark problem in DFT. Such a comparison is of particular interest with regard to the marked differences in the energy-band structure of jellium slabs for these approximations (cf. Ref. 27), which originate from the different character of the HF and x-OEP exchange potentials. The most striking feature is the fact that HF energy bands are perpendicular to the Fermi surface, resulting in a vanishing of the density of states at the Fermi energy. Now, we want to investigate how these differences in the band structure actually affect observable slab quantities, such as the electron density, surface energy, dipole barrier, and work function. In particular, we compare individual contributions to the surface energy and study a localized exchange potential for HF that represents a major exchange contribution.

We consider a neutral spin unpolarized jellium slab of finite width L along the z direction, with two large parallel surfaces on the x-y plane, each of area S. At a final stage, the limit $S \to \infty$ has to be taken. If not otherwise mentioned, atomic units are used throughout our paper.[28] A positive background charge density of the slab,

$$\rho_+(z) = \begin{cases} \rho_0, & |z| \leqslant L/2, \\ 0, & |z| > L/2, \end{cases} \tag{1.1}$$

guarantees charge neutrality.[29] Due to translational symmetry in the directions parallel to the surfaces, the HF normalized orbitals are of the form

$$\psi^{\mathrm{HF}}_{n,\mathbf{k}_\parallel}(\mathbf{r}_\parallel,z) = \frac{e^{i\mathbf{k}_\parallel\cdot\mathbf{r}_\parallel}}{\sqrt{S}}\xi^{\mathrm{HF}}_{n,\mathbf{k}_\parallel}(z), \quad \text{with}$$
$$\int_{-\infty}^{\infty} dz\,\xi^{\mathrm{HF}}_{n,\mathbf{k}_\parallel}(z)^*\xi^{\mathrm{HF}}_{n',\mathbf{k}_\parallel}(z) = \delta_{n,n'}, \tag{1.2}$$

where the perpendicular component $\xi^{\mathrm{HF}}_{n,\mathbf{k}_\parallel}(z)$ of the orbitals depends on the parallel momentum $\mathbf{k}_\parallel$ because of the nonlocal character of the exchange potential, and n is a slab discrete level (SDL) quantum number, which is a consequence of the finite slab size along the z direction and its associated energy quantization. In the limit $S \to \infty$, the slab becomes fully isotropic with respect to the parallel directions and therefore $\xi^{\mathrm{HF}}_{n,k_\parallel}(z)$ depends only on the scalar momentum $k_\parallel$.[27] This kind of coupling is absent in effective one-particle formulations with purely local potentials, such as DFT, where only a local exchange-correlation potential appears in the Kohn-Sham (KS) equations. Thus, for x-OEP normalized orbitals, the ansatz can be further simplified according to

$$\psi^{\mathrm{OEP}}_{n,\mathbf{k}_\parallel}(\mathbf{r}_\parallel,z) = \frac{e^{i\mathbf{k}_\parallel\cdot\mathbf{r}_\parallel}}{\sqrt{S}}\xi^{\mathrm{OEP}}_{n}(z), \quad \text{with}$$
$$\int_{-\infty}^{\infty} dz\,\xi^{\mathrm{OEP}}_{n}(z)^*\xi^{\mathrm{OEP}}_{n'}(z) = \delta_{n,n'}, \tag{1.3}$$

allowing a complete decoupling of the wave function along the x-y plane and the z direction.

The magnitudes of electronic properties typically show a damped oscillatory behavior with periodicity $\lambda_F/2$ with respect to the effective width $L+\delta$ of a jellium slab.[25,27] Here $\lambda_F := 2\pi/k_F$ denotes the Fermi wavelength of the bulk[29] and δ represents a shift parameter that takes into account the leakage of electron density at the jellium surface. For a detailed discussion of the underlying mechanism, we refer to Refs. 30 and 31. We have adjusted the parameter δ for HF calculations at bulk densities $r_s = 2$, 4, and 6, such that integer values of $2(L+\delta)/\lambda_F$ correspond to critical values where an unoccupied band touches the Fermi surface.[27] For $r_s = 2$, 4, and 6, the parameter δ assumes values of 0.327, -1.244, and $-2.947\ a_0$, respectively. Both the HF and x-OEP results presented below were performed under self-consistent conditions. This means that when inserting either HF or x-OEP orbitals in expressions for physical properties, such as the electron density, the electrostatic and exchange potentials, the work function, and the dipole barrier, in all cases the orbitals were the output of associated self-consistent calculations. For details about how these numerical calculations were actually performed, see Ref. 25 (x-OEP) and Ref. 27 (HF).

As an example of these self-consistent calculations, in Fig. 1 we display the band structure of a jellium slab with $r_s = 2$ (left) and $r_s = 6$ (right), in the three different approximations discussed in this work: x-LDA (local density approximation) (upper panel), HF (middle panel), and x-OEP (lower panel). By x-LDA we mean that in the KS equations the actual exchange potential is approximated at this point by the exchange potential of a uniform electron gas with the local density, i.e., $V_x^{\mathrm{LDA}}(z) = -[3\rho_{x-\mathrm{LDA}}(z)/\pi]^{1/3}$. For x-LDA and x-OEP, $\varepsilon_{n,k_\parallel} = \varepsilon_n + k_\parallel^2/2$, with ε_n being the KS eigenvalues that are the output of the self-consistent x-LDA calculation (upper panel), or a self-consistent x-OEP calculation (lower panel). For the HF case, no such decoupling exists for the self-consistent eigenvalues, and $\varepsilon_{n,k_\parallel} = \varepsilon_n(k_\parallel) + k_\parallel^2/2$. There are two interesting features to be noticed from this figure, more clearly displayed in the low-density case ($r_s = 6$). First is the large slope of the occupied HF eigenvalues every time they cross the HF Fermi energy $\varepsilon_F^{\mathrm{HF}}$. This is a well-known

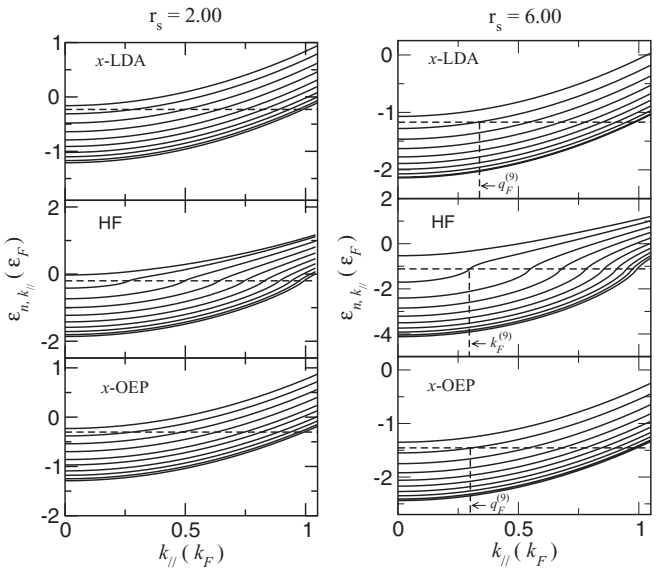

FIG. 1. Self-consistent band structure of a jellium slab with $r_s = 2$ (left), $r_s = 6$ (right), and width $2(L+\delta)/\lambda_F = 8.5$. Upper panel, x-LDA; middle panel, HF; lower panel, x-OEP. Full lines correspond to the dispersion curves $\varepsilon_{n,k_\parallel}$ in each approximation. Horizontal dashed lines correspond to Fermi energies. The zero of energies is at the vacuum level; k_F and ε_F are defined in terms of the background jellium density ρ_0 (Ref. 29). $k_F^{(m)}$ and $q_F^{(m)}$ are defined in the text.

property of the homogeneous three-dimensional electron gas in the HF approximation,[32] which, as discussed above, has been found valid also under much more general conditions.[24] As a consequence, and again as in the electron gas and metallic extended systems, the slab DOS is very small when evaluated at $\varepsilon_F^{\rm HF}$.[33] On the other hand, both x-LDA and x-OEP band structures show no anomalous features at the Fermi level. The second point worth addressing is the very large bandwidth of the HF band structure, as compared with the bandwidth of the x-LDA and x-OEP calculations. By estimating the bandwidth as the difference $\varepsilon_{m,k_\parallel=0} - \varepsilon_{1,k_\parallel=0}$, with m (1) corresponding to the highest (lowest) occupied SDL, the HF bandwidth for the case $r_s = 6$ is about a factor of four greater than the x-LDA and x-OEP bandwidths. The number of occupied SDLs is the same in the three cases, which means that the average energy spacing between SDLs is again about a factor of four greater in the HF band structure. Physically, this anomalous, large HF bandwidth is a consequence of the fact that the HF DOS is very small at the Fermi level, and, by continuity, also small around it; in other words, the HF band structure is such that it needs a larger window of available states in order to accommodate the same number of electrons in the slab, as compared with the other two local approximations to the exchange. Remarkably, as we will see below, this completely different band structure of nonlocal and local treatments of the exchange does not emerge at all in most of the physical slab properties considered here.[34]

II. HF AND x-OEP ELECTRONIC STRUCTURE OF JELLIUM SLABS: COMPARISON OF LOCAL PROPERTIES

In this section, we compare HF and x-OEP local quantities related to the electronic structure of jellium slabs such as the electron densities, the electrostatic potentials, as well as the corresponding exchange potentials. Given the nonlocality of the HF exchange potential, we have used an averaged HF exchange potential due to Slater that can be considered as its natural localization.

A. Electron density, Friedel oscillations, and the electrostatic potential

The HF number-electron density in the limit $S \to \infty$ becomes

$$\rho_{\rm HF}(z) = \frac{1}{\pi}\sum_{n=1}^{m}\int_{k_\parallel \leqslant k_F^{(n)}} k_\parallel dk_\parallel |\xi_{n,k_\parallel}^{\rm HF}(z)|^2, \qquad (2.1)$$

where $k_F^{(n)}$ denotes the Fermi momentum in the parallel directions associated with the discrete quantum number n (see Fig. 1). The integration of $\rho_{\rm HF}(z)$ over the z coordinate yields the charge-neutrality condition

$$\sum_{n=1}^{m}\left[k_F^{(n)}\right]^2 = 2\pi\rho_0 L, \qquad (2.2)$$

which in turn defines the HF Fermi energy $\varepsilon_F^{\rm HF}(L,r_s)$, and through it, $k_F^{(n)}$. The dependence of $\varepsilon_F^{\rm HF}(L,r_s)$ on L and r_s comes from Eq. (2.2), since $\rho_0 \propto r_s^{-3}$. For x-OEP, and due to the decoupling between $k_\parallel$ and n [see Eq. (1.3)], the integral over $k_\parallel$ in Eq. (2.1) can be calculated explicitly as

$$\rho_{x-{\rm OEP}}(z) = \frac{1}{2\pi}\sum_{n=1}^{m}\left[q_F^{(n)}\right]^2\left|\xi_n^{\rm OEP}(z)\right|^2. \qquad (2.3)$$

Here, $q_F^{(n)} = \sqrt{2(\varepsilon_F^{\rm OEP} - \varepsilon_n)}$, with $\varepsilon_F^{\rm OEP}(L,r_s)$ being the x-OEP Fermi energy, and ε_n being the KS x-OEP eigenvalues.[25] The integration of $\rho_{x-{\rm OEP}}(z)$ along z yields the same charge-neutrality condition of Eq. (2.2), but with $k_F^{(n)}$ replaced by $q_F^{(n)}$. In both cases, the sum over index n runs only over occupied slab energy levels ($1 \leqslant n \leqslant m$). The x-LDA slab density $\rho_{x-{\rm LDA}}(z)$ is given by the same expression (2.3), but evaluated with the self-consistent x-LDA orbitals, KS eigenvalues, and Fermi energy.[35]

Figure 2 shows the perpendicular density profile for bulk densities $r_s = 2$ and $r_s = 6$ obtained from HF, x-OEP, and x-LDA calculations for slab widths L given by $2(L+\delta)/\lambda_F = 8.5$. For the self-consistent HF calculations, this value is roughly in the middle between two critical slab widths where a formerly unoccupied band crossed the Fermi surface. It can be seen that the Friedel oscillations near the metal-vacuum interface have considerably smaller amplitude for x-LDA than for HF and x-OEP. Actually, the Friedel oscillations for HF and x-OEP are quite similar. The close similarity between the HF and x-OEP densities have been already discussed in Refs. 20(a) and 23, within the context of calculations of the electronic structure of finite (atomic) systems. A closer inspection shows that the HF oscillations are slightly stronger and decay less rapidly inside the slab than for x-OEP. Plotted in the normalized units ρ_0 and λ_F, it is clear that the relative amplitude of the Friedel oscillations in the electronic density increases with decreasing density.[36] As exchange effects also become larger (in a relative sense) by decreasing the density, one should conclude that the exchange enhances the amplitude (and range) of the oscillations.

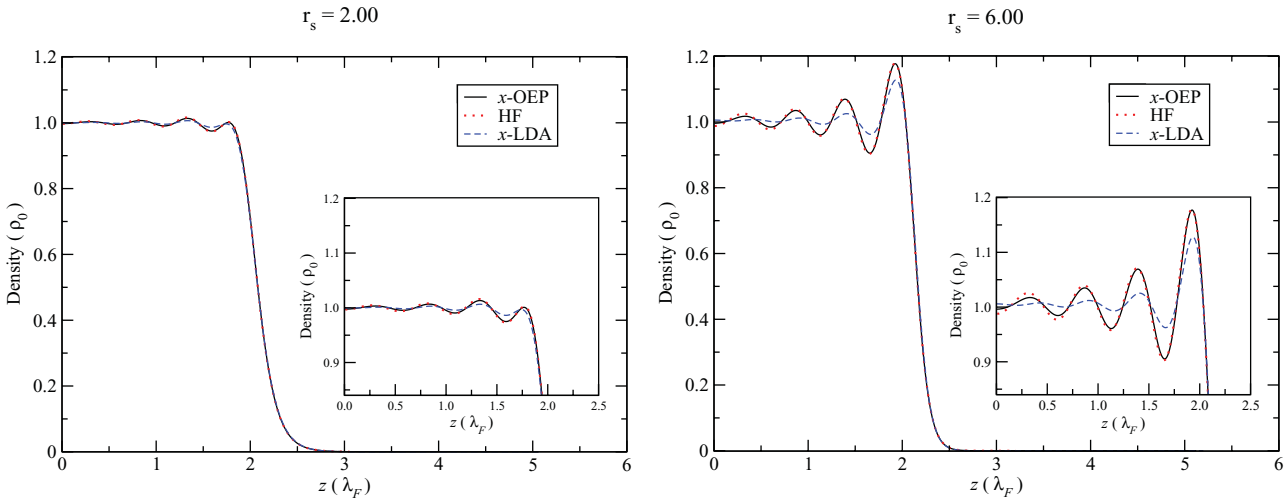

FIG. 2. (Color online) x-OEP (full line), HF (dotted line), and x-LDA (dashed line) density profiles of a jellium slab of width $2(L+\delta)/\lambda_F = 8.5$, for bulk densities $r_s = 2$ (left) and $r_s = 6$ (right). The slab center is at $z = 0$. In all cases, the density has been normalized with the "bulk" density ρ_0. The inset shows an enhanced view of the jellium interface.

The differences in the electron density for x-LDA, HF, and x-OEP reflect themselves in the electrostatic potential,[37]

$$\varphi_i(z) := -2\pi \int_{-\infty}^{\infty} dz' [\rho_i(z') - \rho_+(z')]|z - z'|, \quad (2.4)$$

which represents a convolution of the corresponding electron densities relative to the background charge ($i = x$-LDA, x-OEP, and HF). Figure 3 shows the electrostatic potential for a slab of width L given by $2(L+\delta)/\lambda_F = 8.5$, for bulk densities $r_s = 2$ and $r_s = 6$. It can be seen that the oscillations of the electrostatic potential inside the slab are stronger for HF and x-OEP than for x-LDA. This is easy to understand since the difference $\rho_i(z) - \rho_+(z)$ is the smallest in the $i = x$-LDA case, leading to a $\varphi_{x-\mathrm{LDA}}(z)$ with oscillations of smaller amplitude than HF and x-OEP. On a minor scale, once again the oscillations for HF are slightly stronger than for x-OEP. As compared with the "bulklike" value of the electrostatic potential at the slab center, the amplitude of the oscillations close to the jellium-vacuum interface strongly increases by decreasing the background density.

B. HF versus OEP exchange potentials

The nonlocal character of the HF exchange potential hampers a direct comparison with the corresponding local x-OEP potential. However, it is possible to compare an important part of it, as introduced by Slater[3] as a local approximation of the HF exchange. Following Kleinman,[38] we denote it as the *average Fock approximation* (AFA), in order to avoid possible confusion with other local exchange approximations attributed to Slater. For a general closed-shell system, the AFA exchange potential is given by

$$V_{\mathrm{AFA}}(\mathbf{r}) := -\frac{2}{\rho(\mathbf{r})} \sum_{\alpha,\beta}^{\mathrm{occ}} \int d^3r' \psi_\alpha^*(\mathbf{r})\psi_\beta(\mathbf{r}) \times \frac{1}{|\mathbf{r} - \mathbf{r}'|} \psi_\beta^*(\mathbf{r}')\psi_\alpha(\mathbf{r}'), \quad (2.5)$$

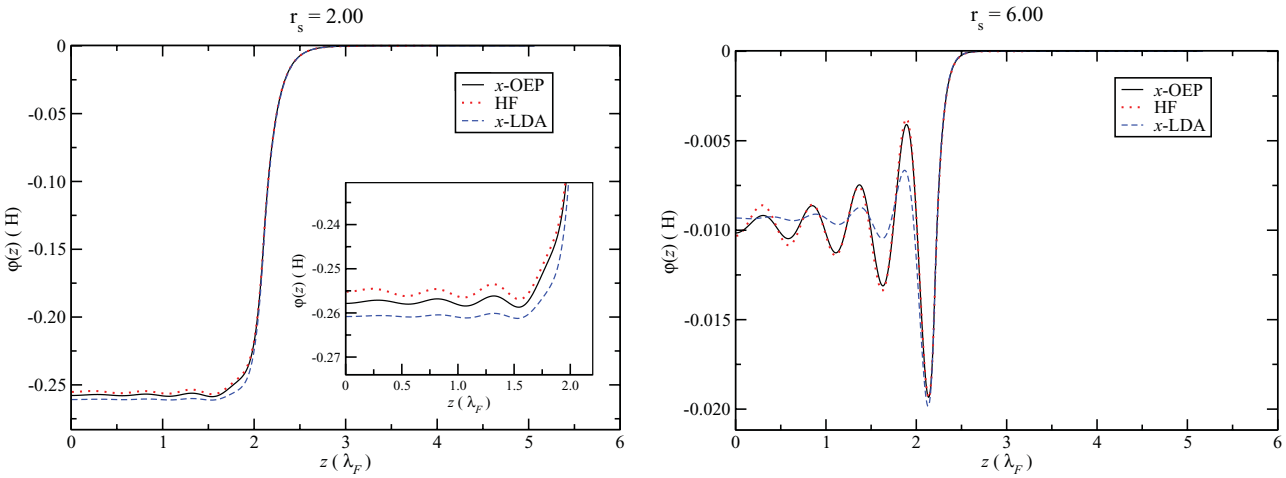

FIG. 3. (Color online) x-OEP (full line), HF (dotted line), and x-LDA (dashed line) electrostatic potentials of a jellium slab of width $2(L+\delta)/\lambda_F = 8.5$, for bulk densities $r_s = 2$ (left) and $r_s = 6$ (right). The inset shows an enhanced view of the vacuum-jellium interface.

with $\psi_\alpha(\mathbf{r})$ being generic three-dimensional orbitals, and $\rho(\mathbf{r})$ being their associated density. By replacing the jellium HF orbitals of Eq. (1.2) in $V_{\rm AFA}(\mathbf{r})$, one obtains

$$V_{\rm AFA}^{\rm HF}(z) = -\frac{1}{4\pi^3\rho_{\rm HF}(z)}\sum_{n,n'=1}^{m}\int_{k_\parallel\leqslant k_F^{(n)}} d^2k_\parallel \int_{k_\parallel{}'\leqslant k_F^{(n')}} d^2k_\parallel{}' \times \int_{-\infty}^{\infty} dz'\xi_{n,k_\parallel}^{\rm HF}(z)^*\xi_{n',k_\parallel'}^{\rm HF}(z) \times \frac{e^{-|\mathbf{k}_\parallel-\mathbf{k}_\parallel'|\,|z-z'|}}{|\mathbf{k}_\parallel-\mathbf{k}_\parallel'|}\xi_{n',k_\parallel'}^{\rm HF}(z')^*\xi_{n,k_\parallel}^{\rm HF}(z'). \quad (2.6)$$

However, the replacement of the x-OEP jellium orbitals of Eq. (1.3) in $V_{\rm AFA}(\mathbf{r})$ yields[39]

$$V_{\rm AFA}^{x-{\rm OEP}}(z) = -\sum_{n,n'=1}^{m}\frac{\xi_n^{\rm OEP}(z)^*\xi_{n'}^{\rm OEP}(z)}{\pi\rho_{x-{\rm OEP}}(z)}\int_{-\infty}^{\infty} dz'\xi_{n'}^{\rm OEP}(z')^* \times \frac{g\left(q_F^{(n)}\Delta z, q_F^{(n')}\Delta z\right)}{\Delta z^3}\xi_n^{\rm OEP}(z'), \quad (2.7)$$

with $\Delta z = |z-z'|$, and

$$g(s,s') = ss'\int_0^\infty \frac{J_1(st)J_1(s't)}{t\sqrt{1+t^2}}dt, \quad (2.8)$$

where J_1 denotes the cylindrical Bessel function of the first order. Despite its original definition in terms of occupied orbitals, AFA can be considered as a functional derivative of an exchange energy functional with respect to the electron density.[38] On the other hand, for the local x-OEP potential, the following well-known decomposition will be used in our analysis later on:[40]

$$V_x(z) = V_{x,1}(z) + V_{x,2}(z), \quad (2.9)$$

where

$$V_{x,1}(z) = \sum_{n=1}^{m}\frac{\left(q_F^{(n)}\right)^2\left|\xi_n^{\rm OEP}(z)\right|^2}{4\pi\rho_{x-{\rm OEP}}(z)}\left\{u_x^n(z) + \Delta\overline{V}_x^n + {\rm c.c.}\right\}, \quad (2.10)$$

and

$$V_{x,2}(z) = -\frac{1}{2\pi\rho_{x-{\rm OEP}}(z)}\sum_{n=1}^{m}\left(\varepsilon_F^{\rm OEP}-\varepsilon_n\right)\left[\left(q_F^{(n)}\right)^2\Psi_n(z) \times \xi_n^{\rm OEP}(z)^* + \Psi_n'(z)\xi_n'^{\rm OEP}(z)^* + {\rm c.c.}\right], \quad (2.11)$$

with primes denoting derivatives with respect to the z coordinate. Also,

$$u_x^n(z) = \frac{4\pi}{S\left(q_F^{(n)}\right)^2\xi_n^{\rm OEP}(z)^*}\frac{\delta E_x}{\delta\xi_n^{\rm OEP}(z)} = -\frac{2}{\left(q_F^{(n)}\right)^2}\sum_{n'=1}^{m}\frac{\xi_{n'}^{\rm OEP}(z)^*}{\xi_n^{\rm OEP}(z)^*} \times \int_{-\infty}^{\infty} dz'\frac{\xi_n^{\rm OEP}(z')^* g\left(q_F^{(n)}\Delta z, q_F^{(n')}\Delta z\right)\xi_{n'}^{\rm OEP}(z')}{(\Delta z)^3}, \quad (2.12)$$

and

$$\Psi_n(z) = \sum_{n'(\neq n)}\frac{\xi_{n'}^{\rm OEP}(z)}{(\varepsilon_n-\varepsilon_{n'})}\int_{-\infty}^{\infty} dz'\xi_{n'}^{\rm OEP}(z')^*\Delta V_x^n(z')\xi_n^{\rm OEP}(z'). \quad (2.13)$$

Here, $\Delta V_x^n(z) := V_x(z) - u_x^n(z)$, and mean values are defined as $\overline{O}^n := \int dz\xi_n(z)^* O^n(z)\xi_n(z)$. This set of equations plus the constraint $\Delta\overline{V}_x^m = 0$ completely determines $V_x(z)$. In the standard literature, the $u_x^n(z)$ are denoted as the orbital-dependent exchange potentials, and the $\Psi_n(z)$ are denoted as the (exchange) "shifts," as they can be physically interpreted as the first-order corrections of the x-OEP KS eigenfunctions $\xi_n^{\rm OEP}(z)$ under the perturbation $\Delta V_x^n(z)$.[41] If the shifts $\Psi_n(z)$ are (arbitrarily) forced to be identically equal to zero, then the only term that survives is $V_{x,1}(z)$. This is exactly the KLI approximation, which brings the identification $V_{x,1}(z) = V_x^{\rm KLI}(z)$.[42] Finally, by neglecting the contribution proportional to $\Delta\overline{V}_x^n$ in the definition of $V_{x,1}(z)$, it reduces to the $V_{\rm AFA}^{x-{\rm OEP}}(z)$ defined previously. From this point of view, $V_{\rm AFA}^{x-{\rm OEP}}(z)$ [and also $V_{\rm AFA}^{\rm HF}(z)$] may be considered as the leading contribution to the full exchange potential as given in Eq. (2.9).

Figure 4 shows the profile of $V_{\rm AFA}^{\rm HF}(z)$, $V_{\rm AFA}^{x-{\rm OEP}}(z)$, and $V_x(z)$ for bulk densities $r_s = 2$ and $r_s = 6$, obtained from the HF and x-OEP self-consistent calculations for a slab of width given by $2(L+\delta)/\lambda_F = 8.5$. It can be seen that the AFA exchange potentials obtained with the HF and x-OEP orbitals are very similar. On the other hand, $V_x(z)$ is less deep than the other two potentials, as they clearly approach different limiting values in the region close to the slab center ($z \sim 0$). These different limiting values are easily obtained in the truly bulklike limit of $z \to -\infty$, corresponding to a slab infinitely wide. In this case,[43]

$$V_{\rm AFA}^{\rm HF}(z\to-\infty) = V_{\rm AFA}^{x-{\rm OEP}}(z\to-\infty) = -\frac{3}{4}\left(\frac{18}{\pi^2}\right)^{1/3}\frac{1}{r_s}, \quad (2.14)$$

and[44]

$$V_x(z\to-\infty) = -\frac{1}{2}\left(\frac{18}{\pi^2}\right)^{1/3}\frac{1}{r_s}. \quad (2.15)$$

Note that $V_{\rm AFA}^{\rm HF}(z\to-\infty) = V_{\rm AFA}^{x-{\rm OEP}}(z\to-\infty) = (3/2)V_x(z\to-\infty)$. For $r_s = 2$, we obtain $V_{\rm AFA}(z\to-\infty) \simeq -0.458$ H, $V_x(z\to-\infty) \simeq -0.305$ H, while for $r_s = 6$, $V_{\rm AFA}(z\to-\infty) \simeq -0.153$ H, $V_x(z\to-\infty) \simeq -0.102$ H. These bulklike values agree reasonably well with the values of the three exchange potentials for the region close to the slab center. However, the two AFA exchange potentials are much closer to their limiting bulk values than $V_x(z)$. As discussed elsewhere, $V_x(z)$ is much more sensitive to the finite slab size than the other two, with the difference stemming mainly from the different boundary conditions that they satisfy.[25] Besides this difference in strength, inside the slab $V_x(z)$ shows slightly stronger oscillations than the AFA potentials. Asymptotically, far on the vacuum side ($z \gg \lambda_F, L$), all three potentials exactly decay as $-1/z$. For $V_{\rm AFA}^{x-{\rm OEP}}(z)$ and $V_x(z)$, this has been shown in Ref. 26; for $V_{\rm AFA}^{\rm HF}(z)$, see Appendix A. Note that at the leading order, this asymptotic limit is "universal," that is, it is valid for slabs of any size and density. The slab material dependence only appears in terms beyond the quoted leading order.

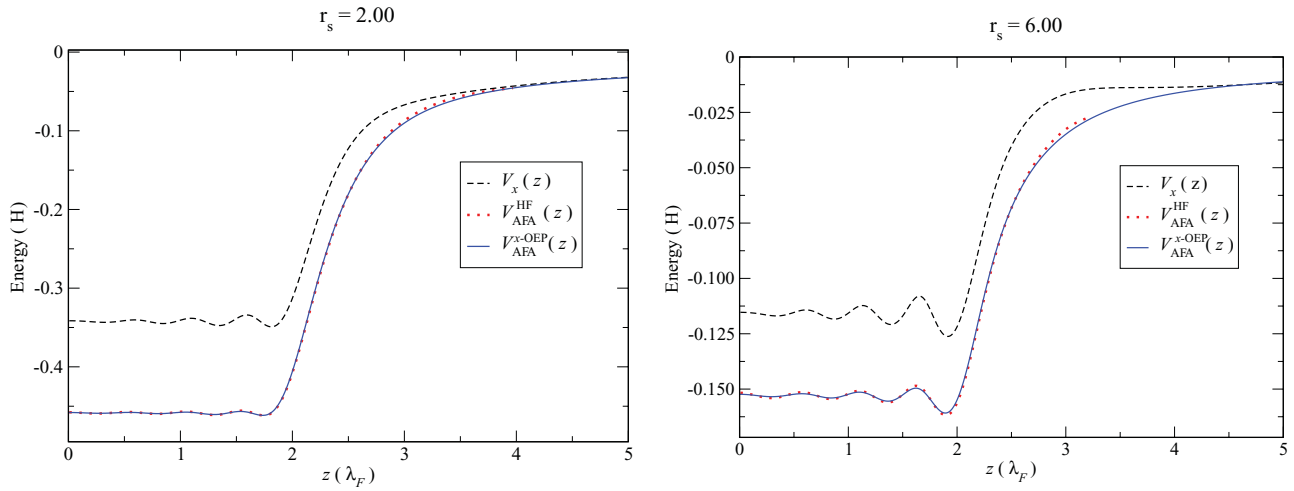

FIG. 4. (Color online) Slater's AFA exchange potential calculated with HF [$V_{\rm AFA}^{\rm HF}(z)$, dotted line] and x-OEP [$V_{\rm AFA}^{x-{\rm OEP}}(z)$, full line] occupied orbitals for a jellium slab of width L with $2(L+\delta)/\lambda_F = 8.5$, for bulk densities $r_s = 2$ (left) and $r_s = 6$ (right). For comparison, the full x-OEP potential $V_x(z)$ (dashed line) is shown.

III. SURFACE ENERGIES, DIPOLE BARRIERS, AND WORK FUNCTIONS

Our comparative study of the electron number density, electrostatic and AFA exchange potentials revealed a good agreement between the HF and x-OEP approximations for these local properties. It remains to be seen whether global properties of jellium slabs agree as well. We have calculated the surface energy $\sigma^i(L,r_s)$ of a jellium slab ($i = x$-LDA, x-OEP, HF) according to the formula[25,27]

$$\sigma^i(L,r_s) := \lim_{S\to\infty} \frac{E^i_{\rm slab}(L,r_s) - E_{\rm bulk}(L,r_s)}{2S}, \qquad (3.1)$$

and considered various contributions to it separately.[45] Here, $E^i_{\rm slab}(L,r_s)$ is the total ground-state energy for a slab of width L and parameter density r_s, and $E^i_{\rm slab}(L, r_s) = E^i_{{\rm slab},K}(L,r_s) + E^i_{{\rm slab},el}(L,r_s) + E^i_{{\rm slab},x}(L,r_s)$, with $E^i_{{\rm slab},K}(L,r_s)$, $E^i_{{\rm slab},el}(L,r_s)$, and $E^i_{{\rm slab},x}(L,r_s)$ being the kinetic (K), electrostatic (el), and exchange (x) contributions to the slab total energy, respectively.[25,27] $E_{\rm bulk}(L,r_s)$ is the total ground-state bulk energy, which is proportional to the size of the system ($\propto LS$).[45] Under this splitting, Eq. (3.1) may in turn be written as

$$\sigma^i(L,r_s) = \sigma^i_K(L,r_s) + \sigma^i_{el}(L,r_s) + \sigma^i_x(L,r_s), \qquad (3.2)$$

where $\sigma^i_K(L,r_s)$ is the kinetic contribution to the surface energy, $\sigma^i_{el}(L,r_s)$ is the electrostatic surface energy due to all noncompensated positive and negative charge distributions in the slab, and $\sigma^i_x(L,r_s)$ is the exchange contribution to the surface energy. From elementary physical arguments, it follows that $\sigma^i_K(L,r_s) < 0$, while $\sigma^i_{el}(L,r_s)$ and $\sigma^i_x(L,r_s)$ are both positive.[46] The results for our favorite slab width L given by $2(L+\delta)/\lambda_F = 8.5$ for bulk densities $r_s = 2, 4$, and 6 are listed in Table I. It can be seen that the surface energy decreases in the order $\sigma^{x-{\rm LDA}}(L,r_s) > \sigma^{x-{\rm OEP}}(L,r_s) > \sigma^{\rm HF}(L,r_s)$ for all three densities. It is interesting to point out that in all of the cases we have studied, $\sigma^{x-{\rm OEP}}(L,r_s)$ is slightly higher than $\sigma^{\rm HF}(L,r_s)$. This is just a manifestation of the fact that $E^{x-{\rm OEP}}_{\rm slab} \geqslant E^{\rm HF}_{\rm slab}$, due to the extra constraint that is present in the OEP variational optimization derivation of $V_x(z)$, as compared with the HF case. The fact that our calculations are able to resolve this minute difference between the x-OEP and HF total energies, which are two very large numbers compared to the surface energies, is an indication of their high accuracy. The individual contributions obey regular patterns as well, i.e., exchange contribution $\sigma_x^{x-{\rm LDA}}(L,r_s) > \sigma_x^{x-{\rm OEP}}(L,r_s) > \sigma_x^{\rm HF}(L,r_s)$ and kinetic energy $\sigma_K^{x-{\rm LDA}}(L,r_s) < \sigma_K^{x-{\rm OEP}}(L,r_s) < \sigma_K^{\rm HF}(L,r_s)$. In summary, the differences in the surface energy between the three approximations are rather small.

Another quantity of interest is the dipole barrier[36] for jellium slabs,

$$\Delta\Phi_i := \varphi_i(z\to\infty) - \varphi_i(z=0) = 4\pi \int_0^\infty dz\,[\rho_i(z) - \rho_+(z)]\,z\,dz, \qquad (3.3)$$

TABLE I. Surface energy $\sigma(L,r_s)$, dipole barrier $\Delta\Phi(L,r_s)$, and work function $W(L,r_s)$ of jellium slabs at bulk electron densities $r_s = 2$, $r_s = 4$, and $r_s = 6$, with slab widths (L) given by $2(L+\delta)/\lambda_F = 8.5$. Various contributions to the surface energy are given separately: σ_x (exchange), σ_K (kinetic), and σ_{es} (electrostatic).

	σ_x (erg/cm^2)	σ_K (erg/cm^2)	σ_{es} (erg/cm^2)	σ (erg/cm^2)	$\Delta\Phi$ (eV)	W (eV)
			$r_s = 2$, $\delta = 0.327\ a_0$			
x-LDA	2756	−5737	1405	−1576	7.09	2.88
x-OEP	2686	−5611	1338	−1587	7.01	3.80
HF	2637	−5571	1323	−1611	6.94	2.48
			$r_s = 4$, $\delta = -1.244\ a_0$			
x-LDA	183	−170	47	60	1.14	2.17
x-OEP	167	−156	45	56	1.15	2.72
HF	154	−152	45	47	1.14	2.02
			$r_s = 6$, $\delta = -2.947\ a_0$			
x-LDA	33.1	−13.5	9.2	28.8	0.25	1.63
x-OEP	25.8	−10.6	11.7	26.9	0.28	2.03
HF	19	−8	12	23	0.28	1.55

which corresponds to the difference of the electrostatic potential at infinity (far on the vacuum side) and at the center of the slab. The HF, x-OEP, and x-LDA dipole barriers are in good agreement for different bulk densities, as can be seen from Table I, which means that the much stronger Friedel oscillations of the electrostatic potential in HF and x-OEP compared with x-LDA do not essentially affect this global quantity.

It has already been mentioned in Sec. I that the HF band structure differs significantly from the x-OEP and x-LDA band structures. The most sensitive quantity to probe the electronic structure close to the Fermi surface is the work function that represents the energy necessary to remove an electron to infinity. Since relaxation effects are negligible for an infinitely extended slab, Koopmans' theorem can be applied to obtain the HF work function without further approximation.[47] On the other side, in the context of DFT, exists the "ionization-potential theorem," according to which the energy of the highest occupied KS orbital (usually denoted HOMO) equals the negative of the ionization potential; this theorem is exact for the exact exchange-correlation functional.[48] And since the ionization potential is the equivalent of the work function for a solid-state system, in both cases the work function therefore corresponds to minus the corresponding Fermi energies, i.e.,

$$W^i(L,r_s) = -\varepsilon_F^i(L,r_s), \tag{3.4}$$

with $i = x$-LDA, HF, and x-OEP. Through the Fermi-level energies, the slab work function becomes slab-size and density dependent. Contrary to the other quantities discussed before, we observed large differences among all three approximations. In particular, the difference between HF and x-OEP work functions becomes very large, as can be seen in Table I. To the best of our knowledge, this is the largest discrepancy between HF and x-OEP properties that has been observed so far. For example, atomic HF and x-OEP ionization energies reported in the literature[49] are in good agreement with each other.

In order to see how the difference between HF and x-OEP work functions depends on the slab width, we performed calculations at other values of L for the bulk density $r_s = 4$ as well. The results are listed in Table II; here slab widths alternatively correspond to critical values at which a new SDL becomes occupied and intermediate values at which no changes in the number of occupied SDLs occur in their close neighborhood. As before, surface energies and dipole barriers agree well for HF and x-OEP, independent of the slab width. It can be seen that the HF work function remains almost constant for the slab widths under consideration. This is not, however, the case for the x-OEP work function $W^{x-\mathrm{OEP}}(L,r_s)$, which strongly oscillates, as can be seen from Fig. 5, where we have plotted $W^{x-\mathrm{OEP}}(L,r_s)$ versus the slab width. The abrupt change displayed by $W^{x-\mathrm{OEP}}(L,r_s)$ every time $2(L+\delta)/\lambda_F$ is close to an integer value is associated with the change in the number of occupied SDLs in the x-OEP electronic band structure. This discontinuous change is not present either in the HF work function or in the x-LDA work function, which presents a much smaller dependence on the slab size.[50]

In order to obtain a better insight into this phenomenon, we can proceed as follows. A convenient definition for the HF work function is

$$W^{\mathrm{HF}}(L,r_s) = -\varepsilon_{m,k_F^{(m)}}(L,r_s). \tag{3.5}$$

The index m corresponds to the number of occupied SDLs, and as $\varepsilon_{1,k_F^{(1)}}(L,r_s) = \varepsilon_{2,k_F^{(2)}}(L,r_s) = \cdots = \varepsilon_{m,k_F^{(m)}}(L,r_s) = \varepsilon_F^{\mathrm{HF}}(L,r_s)$, this is equivalent to $W^{\mathrm{HF}}(L,r_s) = -\varepsilon_F^{\mathrm{HF}}(L,r_s)$, as above. After a few manipulations with the HF slab Schrödinger equation, we obtain

$$W^{\mathrm{HF}}(L,r_s) = W_K^{\mathrm{HF}}(L,r_s) + W_{el}^{\mathrm{HF}}(L,r_s) + W_x^{\mathrm{HF}}(L,r_s), \tag{3.6}$$

TABLE II. Surface energy $\sigma(L,r_s)$, dipole barrier $\Delta\Phi(L,r_s)$, and work function $W(L,r_s)$ of jellium slabs at bulk electron density $r_s = 4$ with slab widths (L) given by $2(L+\delta)/\lambda_F$ with $\delta = -1.244\ a_0$. Various contributions to the surface energy are given separately: σ_x (exchange), σ_K (kinetic), and σ_{es} (electrostatic).

	σ_x (erg/cm^2)	σ_K (erg/cm^2)	σ_{es} (erg/cm^2)	σ (erg/cm^2)	$\Delta\Phi$ (eV)	W (eV)
			$2(L+\delta)/\lambda_F = 9.5$			
x-OEP	166	−156	45	55	1.12	2.67
HF	147	−147	49	49	1.09	2.01
			$2(L+\delta)/\lambda_F = 10.0$			
x-OEP	153	−149	45	49	1.12	2.86
HF	134	−142	48	40	1.08	1.99
			$2(L+\delta)/\lambda_F = 10.5$			
x-OEP	164	−155	45	54	1.13	2.63
HF	146	−147	49	48	1.12	2.00
			$2(L+\delta)/\lambda_F = 11.0$			
x-OEP	153	−149	45	49	1.07	2.80
HF	133	−141	49	41	1.07	1.99
			$2(L+\delta)/\lambda_F = 11.5$			
x-OEP	163	−154	45	54	1.11	2.60
HF	146	−147	49	48	1.09	2.01

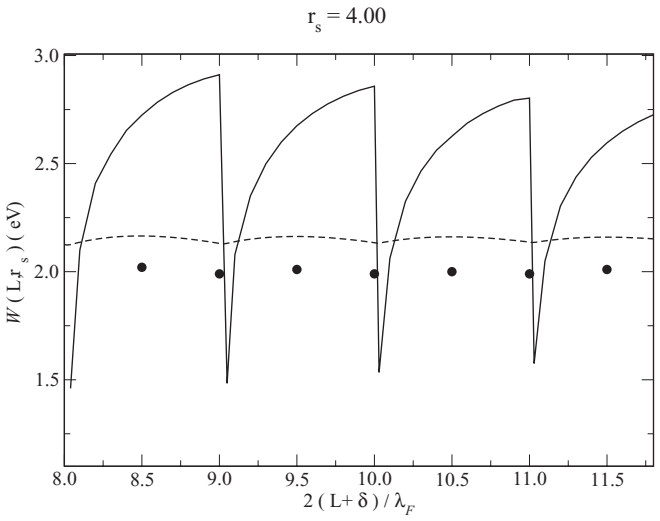

FIG. 5. x-OEP (full line) and x-LDA (dashed line) work functions of a jellium slab vs slab width $2(L+\delta)/\lambda_F$, with $\delta = -1.244\ a_0$, for bulk density $r_s = 4$. Values of the HF work function $W^{\mathrm{HF}}(L,4)$ are given at selected slab widths (dots).

with

$$W_K^{\rm HF}(L,r_s) = \frac{1}{2}\int_{-\infty}^{\infty} dz \xi^{\rm HF}_{m,k_F^{(m)}}(z)^* \frac{d^2}{dz^2}\xi^{\rm HF}_{m,k_F^{(m)}}(z) - \frac{1}{2}\left(k_F^m\right)^2,$$

$$W_{el}^{\rm HF}(L,r_s) = -\int_{-\infty}^{\infty} dz \varphi_{\rm HF}(z)\left|\xi_{m,k_F^{(m)}}(z)\right|^2,$$

$$W_x^{\rm HF}(L,r_s) = \sum_{n=1}^{m}\int_{k'_\parallel \leqslant k_F^{(n)}} d^2k_\parallel{}' \int_{-\infty}^{\infty} dz \int_{-\infty}^{\infty} dz' \xi^{\rm HF}_{m,k_F^{(m)}}(z)^* \times \xi^{\rm HF}_{n,k'_\parallel}(z)\xi^{\rm HF}_{m,k_F^{(m)}}(z')\xi^{\rm HF}_{n,k'_\parallel}(z)^* \frac{e^{-|\mathbf{k}_\parallel-\mathbf{k}'_\parallel|_*\,|z-z'|}}{2\pi|\mathbf{k}_\parallel-\mathbf{k}'_\parallel|_*}, \quad (3.7)$$

and $|\mathbf{k}_\parallel - \mathbf{k}'_\parallel|_* = |(k_F^{(m)})^2 - 2k_F^{(m)}k'_\parallel\cos\theta + k'^2_\parallel|^{1/2}$.

On the other hand, considering that the x-OEP KS equation is given by

$$\left[-\frac{1}{2}\frac{d^2}{dz^2} + V_{\rm KS}(z)\right]\xi_n^{\rm OEP}(z) = \varepsilon_n\xi_n^{\rm OEP}(z), \quad (3.8)$$

with $V_{\rm KS}(z) = \varphi_{x-{\rm OEP}}(z) + V_x(z)$, we obtain

$$\varepsilon_n = \int_{-\infty}^{\infty} dz \xi_n^{\rm OEP}(z)^* \times\left[-\frac{1}{2}\frac{d^2}{dz^2} + \varphi_{x-{\rm OEP}}(z) + V_x(z)\right]\xi_n^{\rm OEP}(z). \quad (3.9)$$

Using this equation for the case $n = m$, the x-OEP work function now is

$$W^{x-{\rm OEP}}(L,r_s) = -\varepsilon_F^{\rm OEP}(L,r_s) = -\left[\varepsilon_m(L,r_s) + \frac{q_F^{(m)2}}{2}\right] = W_K^{x-{\rm OEP}}(L,r_s) + W_{el}^{x-{\rm OEP}}(L,r_s) + W_x^{x-{\rm OEP}}(L,r_s). \quad (3.10)$$

Here, $W_K^{x-{\rm OEP}}(L,r_s)$ and $W_{el}^{x-{\rm OEP}}(L,r_s)$ are given by the same expressions as in Eq. (3.7), but replacing the HF orbitals by the x-OEP orbitals, that is, $k_F^{(m)}$ by $q_F^{(m)}$ and $\varphi_{\rm HF}(z)$ by $\varphi_{x-{\rm OEP}}(z)$. Besides,

$$W_x^{x-{\rm OEP}}(L,r_s) = -\int_{-\infty}^{\infty} dz\left|\xi_m^{\rm OEP}(z)\right|^2 V_x(z). \quad (3.11)$$

Now, for $n = m$, we have the important x-OEP boundary condition,[40]

$$\overline{V}_x^m = \overline{u}_x^m \rightarrow \int_{-\infty}^{\infty} dz\left|\xi_m^{\rm OEP}(z)\right|^2 V_x(z) = \int_{-\infty}^{\infty} dz\left|\xi_m^{\rm OEP}(z)\right|^2 u_x^m(z). \quad (3.12)$$

Using this condition in Eq. (3.11) to eliminate $V_x(z)$ in favor of $u_x^m(z)$, we obtain

$$W_x^{x-{\rm OEP}}(L,r_s) = -\int_{-\infty}^{\infty} dz\left|\xi_m^{\rm OEP}(z)\right|^2 u_x^m(z). \quad (3.13)$$

It is worth addressing here that this equation is *only* valid for the highest occupied OEP SDL. Its usefulness lies in the fact that while for $V_x(z)$ we do not have an explicit expression, for $u_x^m(z)$ we do have an explicit expression, in terms of the self-consistent KS OEP orbitals [see Eq. (2.12)].

The difference between both work functions is then given as

$$W^{x-{\rm OEP}}(L,r_s) - W^{\rm HF}(L,r_s) = W_K^{x-{\rm OEP}}(L,r_s) - W_K^{\rm HF}(L,r_s) + W_{el}^{x-{\rm OEP}}(L,r_s) - W_{el}^{\rm HF}(L,r_s) + W_x^{x-{\rm OEP}}(L,r_s) - W_x^{\rm HF}(L,r_s). \quad (3.14)$$

Results for the HF and x-OEP work functions for several slab sizes and background densities are given in Table III. The first two rows correspond to narrow slabs, with only one occupied SDL ($m = 1$), both in the HF and x-OEP approximations. The last three rows, corresponding to wider slab sizes, have a band structure with nine occupied SDLs ($m = 9$), once again both in the HF and x-OEP approximations. The values for the different contributions to the work function show a general trend: $W_K^{\rm HF}(L,r_s)$ is quite similar to $W_K^{x-{\rm OEP}}(L,r_s)$ in all cases, and the same applies to $W_{el}^{\rm HF}(L,r_s)$ and $W_{el}^{x-{\rm OEP}}(L,r_s)$. On the other hand, the differences between $W_x^{\rm HF}(L,r_s)$ and $W_x^{x-{\rm OEP}}(L,r_s)$ are noticeable, and account for most of the differences between both work functions (see last two columns of the table). In terms of Eq. (3.14), this corresponds to an almost complete cancellation of the first line on the right-hand side (rhs). In order to understand why $W_x^{\rm HF}(L,r_s)$ and $W_x^{x-{\rm OEP}}(L,r_s)$ are very different, it is important to note that $W_x^{x-{\rm OEP}}(L,r_s)$ is mainly responsible for the strong finite-size oscillations in $W^{x-{\rm OEP}}(L,r_s)$. As explained in detail in Appendix B, $W_x^{x-{\rm OEP}}(L,r_s)$ has abrupt (discontinuous) changes as a function of L every time a new SDL becomes occupied (or emptied). This feature is absent in $W_x^{\rm HF}(L,r_s)$, and explains the large differences between both work functions allowed above. It also largely explains the noticeable differences between $W^{x-{\rm OEP}}(L,r_s)$ and $W^{\rm HF}(L,r_s)$ shown in Fig. 5. Also, looking at the corresponding expressions for $W_x^{\rm HF}(L,r_s)$ [Eq. (3.7)] and for $W_x^{x-{\rm OEP}}(L,r_s)$ [Eq. (3.13)], it is clear that another difference comes from the fact that in the HF case, there is an intrinsic coupling between the parallel and perpendicular degrees of freedom, which does not exist in the x-OEP case.

The general results discussed here, namely, $\varepsilon_F^{\rm HF} = -W^{\rm HF} \neq \varepsilon_F^{\rm OEP} = -W^{x-{\rm OEP}}$, do not contradict the result found in Ref. 18 for finite systems, which amounts to the establishment of the equivalence of the HOMO energies corresponding to either the HF or x-OEP Hamiltonians. However, in both cases, the expectation values of the corresponding Hamiltonians are taken by using the same KS x-OEP HOMO orbitals. In our case, this will allow us to replace the HF orbitals $\xi^{\rm HF}_{m,k_F^{(m)}}(z)$ by the x-OEP orbitals $\xi_m^{\rm OEP}(z)$ in Eq. (3.7). So, the expression in Eq. (3.7) reduces in to the corresponding magnitudes in Eq. (3.10), and we arrive at the same conclusion as in Ref. 18.

While we can explain why we have an important discrepancy between $W^{x-{\rm OEP}}(L,r_s)$ and $W^{\rm HF}(L,r_s)$ for narrow or not-quite-wide slabs ($L \sim \lambda_F$), we argue now that they approach a very similar asymptotic value in the limit of wide slabs ($L \gg \lambda_F$), as shown by the $W^{x-{\rm OEP}}$ values given between parentheses in Table III. As explained in Ref. 25, they correspond to the infinite-width slab extrapolated x-OEP work functions. Considering the tiny slab-size oscillations shown by $W^{\rm HF}(L,r_s)$ in Fig. 5, they can also be considered as

TABLE III. Comparison of HF and x-OEP work functions for selected slab sizes and densities. Extrapolated semi-infinite ($L \gg \lambda_F$) values of the x-OEP work function are given as superscript numbers between parentheses for the three densities considered.[25]

	HF				x-OEP					
$\frac{2(L+\delta)}{\lambda_F}, r_s$	W_K (eV)	W_{el} (eV)	W_x (eV)	W (eV)	W_K (eV)	W_{el} (eV)	W_x (eV)	W (eV)	$W_x^{x-\mathrm{OEP}} - W_x^{\mathrm{HF}}$ (eV)	$W^{x-\mathrm{OEP}} - W^{\mathrm{HF}}$ (eV)
0.15, 2	−3.76	2.68	4.47	3.39	−3.82	2.72	6.96	$5.86^{(2.64)}$	2.49	2.46
0.30, 2	−6.71	3.76	5.99	3.04	−6.82	3.81	9.32	$6.31^{(2.64)}$	3.33	3.27
8.50, 2	−9.59	5.37	6.69	2.47	−9.60	5.36	8.04	$3.80^{(2.64)}$	1.36	1.34
8.50, 4	−2.81	1.08	3.75	2.02	−2.77	1.07	4.42	$2.72^{(2.11)}$	0.67	0.70
8.50, 6	−1.30	0.29	2.56	1.55	−1.28	0.30	3.01	$2.03^{(1.61)}$	0.46	0.47

good estimates of the HF work function in the large-width slab limit. Proceeding in this way, the difference $W^{x-\mathrm{OEP}}(L \to \infty, r_s) - W^{\mathrm{HF}}(L \to \infty, r_s)$ may be estimated to be 0.16 eV ($r_s = 2$), 0.09 eV ($r_s = 4$), and 0.06 eV ($r_s = 6$). Given the fact that in both cases the values adopted for $W^{x-\mathrm{OEP}}(L \gg \lambda_F, r_s)$ and $W^{\mathrm{HF}}(L \gg \lambda_F, r_s)$ are just estimates of the true asymptotic values, the possibility that both are the same in the semi-infinite limit cannot be disregarded. This is of course a conjecture that can only be answered unambiguously by performing the corresponding x-OEP and HF calculations in a semi-infinite geometry.[51]

IV. CONCLUSIONS

Orbital-dependent exchange-correlation functionals play a major role in recent developments of DFT aiming to overcome essential shortcomings of the well-established LDA and density-gradient corrected functionals. In principle, these orbital-dependent functionals can be applied in different manners. For instance, for the exchange contribution, two well-known alternatives exist. The first alternative is to optimize the exchange functional with respect to the orbitals yielding the nonlocal HF exchange potential that can be directly added to the KS equation. The second alternative is to take the functional derivative with respect to the density and obtain a corresponding local x-OEP potential. For different reasons, both approaches are computationally more demanding than any standard local approximation to the exchange. Therefore, it is interesting to see what the differences and common features of these two approaches are. Within the present work, we have studied this problem for jellium slabs using the HF and x-OEP approximations. It turned out that for almost all ground-state physical properties under consideration, good agreement has been observed between the HF and x-OEP results. In particular, we have compared the corresponding electronic densities, electrostatic and averaged exchange potentials, dipole barriers, and surface energies. Significant deviations have been observed for the work functions of finite slabs only. This is a special feature of the jellium slab geometry, where the nonlocal character of the HF exchange potential causes a coupling of the momentum parallel to the slab surface with the perpendicular component of the orbitals.

Similarly, the *random phase approximation* (RPA) for the correlation functional can be either applied in a post-DFT manner by taking KS orbitals from some approximate functional, or it can be handled within the OEP scheme generating a corresponding local RPA correlation potential. It will be interesting to further extend our slab exchange-only results to include correlation effects along these lines, and compare both approaches once again.

APPENDIX A: ASYMPTOTIC BEHAVIOR OF HF-AFA POTENTIAL

In this Appendix, we want to discuss the asymptotic behavior of the HF-AFA exchange potential (2.6) for $z \to \infty$. The occupied HF orbitals decay exponentially in the vacuum region,[52] therefore

$$\frac{e^{-|\mathbf{k}_\parallel - \mathbf{k}'_\parallel|\ |z-z'|}}{|\mathbf{k}_\parallel - \mathbf{k}'_\parallel|} \tag{A1}$$

for $z \to \infty$ is strongly peaked around $|\mathbf{k}_\parallel - \mathbf{k}'_\parallel| = 0$, and $|z - z'| \approx z$ can be used in the integrand, as long as $z \gg L$. It is reasonable to assume then that the orbitals depend smoothly on $\mathbf{k}_\parallel$, which means that we can approximate

$$\begin{aligned} V_{\mathrm{AFA}}^{\mathrm{HF}}(z \to \infty) \approx & -\frac{1}{4\pi^3 \rho(z)} \sum_{n,n'=1}^{m} \int_{k_\parallel \leqslant k_F^{(n)}} d^2k_\parallel \xi_{n,k_\parallel}^{\mathrm{HF}}(z)^* \\ & \times \xi_{n',k_\parallel}^{\mathrm{HF}}(z) \int_{-\infty}^{\infty} dz' \xi_{n,k_\parallel}^{\mathrm{HF}}(z') \xi_{n',k_\parallel}^{\mathrm{HF}}(z')^* \\ & \times \int_{B(\epsilon)} d^2\delta k_\parallel \frac{e^{-|\delta\mathbf{k}_\parallel|\ |z|}}{|\delta\mathbf{k}_\parallel|} \\ \approx & -\frac{1}{2\pi^2 z \rho_{\mathrm{HF}}(z)} \sum_{n=1}^{m} \int_{k_\parallel \leqslant k_F^{(n)}} d^2k_\parallel \left|\xi_{n,k_\parallel}^{\mathrm{HF}}(z)\right|^2 \\ = & -\frac{1}{z}, \end{aligned} \tag{A2}$$

where $\delta\mathbf{k}_\parallel = \mathbf{k}_\parallel - \mathbf{k}'_\parallel$ is confined to a small ball $B(\epsilon)$ of radius $\varepsilon > 0$ around the origin. In passing from the first to the second line, the integration over $\delta\mathbf{k}_\parallel$ has been extended to all two-dimensional wave-vector space, as the exponential factor in the limit $z \to \infty$ automatically filters all $|\delta\mathbf{k}_\parallel|$ values, except the smallest ones. In the last step, we have applied (2.1) for the electron density. Result (A2) coincides, to the leading order, with the asymptotic values of $V_{\mathrm{AFA}}^{x-\mathrm{OEP}}(z)$ and $V_x(z)$.

APPENDIX B: ON THE SOURCE OF THE STRONG QUANTUM-SIZE EFFECT IN THE OEP WORK FUNCTION

For the discussion in the present Appendix, we will slightly modify the notation in Eq. (3.11) as follows:

$$W_x^{x-\mathrm{OEP}}(L^+,r_s) = -\int_{-\infty}^{\infty} dz \left|\xi_m^{\mathrm{OEP}}(z)\right|^2 V_x^+(z), \quad \text{(B1)}$$

with the superscript "+" in L^+ and $V_x^+(z)$ meaning that for this slab size, the $m-$SDL has an infinitesimal occupation, and that the associate exchange potential is $V_x^+(z)$. Similarly, we can consider

$$W_x^{x-\mathrm{OEP}}(L^-,r_s) = -\int_{-\infty}^{\infty} dz \left|\xi_{m-1}^{\mathrm{OEP}}(z)\right|^2 V_x^-(z) \quad \text{(B2)}$$

as the exchange contribution to the work function corresponding to a slab size L^-, whose highest occupied SDL is the $m-1$, and such that L^- is smaller than L^+ by just an infinitesimal amount. $V_x^-(z)$ is the corresponding exchange potential.

According to Eq. (48) in Ref. 25, under these conditions, and for all physically relevant distances, both exchange potentials are related through

$$V_x^+(z) = V_x^-(z) + C_x(m), \quad \text{(B3)}$$

with $C_x(m)$ being an m-dependent constant. By replacing Eq. (B3) in Eq. (B1), one obtains

$$W_x^{x-\mathrm{OEP}}(L^+,r_s) = -\int_{-\infty}^{\infty} dz \left|\xi_m^{\mathrm{OEP}}(z)\right|^2 V_x^-(z) - C_x(m). \quad \text{(B4)}$$

By a comparison of Eqs. (B4) and (B2), one realizes that right at the $m-1 \to m$ SDL transition, the work function has two sources of abrupt change: (i) the change $\xi_{m-1}^{\mathrm{OEP}}(z) \to \xi_m^{\mathrm{OEP}}(z)$ in Eq. (B2), and (ii) the appearance of the constant $C_x(m)$ in Eq. (B4). From the corresponding difference,

$$W_x^{x-\mathrm{OEP}}(L^+,r_s) - W_x^{x-\mathrm{OEP}}(L^-,r_s) = -\int_{-\infty}^{\infty} dz \left[\left|\xi_m^{\mathrm{OEP}}(z)\right|^2 - \left|\xi_{m-1}^{\mathrm{OEP}}(z)\right|^2\right] V_x^-(z) - C_x(m). \quad \text{(B5)}$$

While it is difficult to estimate the size and even the sign of the first term on the rhs of Eq. (B5), the contribution from the second term is negative [since $C_x(m) > 0$], and its magnitude decreases with increasing m, as shown in Fig. 9 of Ref. 25. The abrupt changes in $W^{\mathrm{OEP}}(L,r_s)$ shown in Fig. 5 just follow the same trend, as expected from Eq. (B5). This suggests that the sharp drops are mainly a consequence of the appearance of the contribution related to $C_x(m)$ and not the contribution coming from the first term on the rhs of Eq. (B5). On the other side, good discussions of the weak quantum-size effect (QSE) in jellium slabs may be found in Ref. 50 and references therein. Note, however, that the use of "continuum" exchange-correlation energy functionals in these works leads to a vanishing of the strong discontinuities, as displayed in Eq. (B5), for the x-OEP work function.

[1] E. K. U. Gross, E. Runge, and O. Heinonen, *Many-Particle Theory* (Hilger, London, 1991).
[2] F. Herman, J. P. Van Dyke, and I. B. Ortenburger, Phys. Rev. Lett. **22**, 807 (1969).
[3] J. C. Slater, Phys. Rev. **81**, 385 (1951).
[4] R. G. Parr and W. Yang, *Density-Functional Theory of Atoms and Molecules* (Oxford University Press, London, 1989).
[5] P. Jørgensen and Y. Öhrn, Phys. Rev. A **8**, 112 (1973).
[6] A. D. Becke, J. Chem. Phys. **84**, 4524 (1986); **85**, 7184 (1986).
[7] A. D. Becke, Phys. Rev. A **38**, 3098 (1988).
[8] D. C. Langreth and J. P. Perdew, Solid State Commun. **31**, 567 (1979); Phys. Rev. B **21**, 5469 (1980).
[9] J. P. Perdew and Y. Wang, Phys. Rev. B **33**, 8800(R) (1986); **40**, 3399 (1989).
[10] A. D. Becke, J. Chem. Phys. **96**, 2155 (1992); **97**, 9173 (1992).
[11] W. Kohn and L. J. Sham, Phys. Rev. **137**, A1697 (1965).
[12] A. D. Becke, J. Chem. Phys. **98**, 1372 (1993); **98**, 5648 (1993).
[13] In principle, it would be possible to stay with these hybrid functionals within the realm of the KS implementation of DFT, with a purely local exchange potential. In practice, most of the calculations that use these hybrid functionals are performed with a nonlocal exchange potential (HF-like).
[14] R. T. Sharp and G. K. Horton, Phys. Rev. **30**, 317 (1953).
[15] J. D. Talman and W. F. Shadwick, Phys. Rev. A **14**, 36 (1976).
[16] T. Grabo, T. Kreibich, S. Kurth, and E. K. U. Gross, in *The Strong Coulomb Correlations and Electronic Structure Calculations: Beyond Local Density Approximations*, edited by V. Asimov, (Gordon and Breach, Amsterdam, 2000), p. 203.
[17] S. Kümmel and L. Kronik, Rev. Mod. Phys. **80**, 1 (2008).
[18] J. B. Krieger, Y. Li, and G. J. Iafrate, Phys. Rev. A **45**, 101 (1992).
[19] J. P. Perdew and M. R. Norman, Phys. Rev. B **26**, 5445 (1982).
[20] (a) S. B. Trickey, Phys. Rev. B **30**, 3523 (1984); (b) J. P. Perdew and M. R. Norman, *ibid.* **30**, 3525 (1984).
[21] S. Ivanov and M. Levy, J. Chem. Phys. **119**, 7087 (2003).
[22] A. Görling and M. Ernzerhof, Phys. Rev. A **51**, 4501 (1995).
[23] Y. Li, J. B. Krieger, and G. J. Iafrate, Phys. Rev. A **47**, 165 (1993).
[24] H. J. Monkhorst, Phys. Rev. B **20**, 1504 (1979).
[25] C. M. Horowitz, C. R. Proetto, and J. M. Pitarke, Phys. Rev. B **78**, 085126 (2008).
[26] C. M. Horowitz, L. A. Constantin, C. R. Proetto, and J. M. Pitarke, Phys. Rev. B **80**, 235101 (2009).
[27] H. Luo, W. Hackbusch, H.-J. Flad, and D. Kolb, Phys. Rev. B **78**, 035136 (2008).
[28] Unit of length $a_0 = 0.529$ Å (Bohr radius), unit of energy H = 27.2116 eV (Hartree), unit of mass $m_0 = 9.10956 \times 10^{-28}$ g (electron rest mass).
[29] ρ_0 is given by $\rho_0 = 3/(4\pi r_s^3 a_0^3)$, with r_s being the dimensionless electron-density parameter defined as the radius of a sphere

containing one electron on average and a_0 being the Bohr radius. Convenient units of length, wave vector, and energy for the present system are the Fermi wavelength $\lambda_F = (32\pi^2/9)^{1/3} r_s a_0 \approx 3.724\, r_s a_0$, the Fermi wave vector $k_F = 2\pi/\lambda_F = (9\pi/4)^{1/3}/(r_s a_0)$, and the Fermi energy $\varepsilon_F = \hbar^2 k_F^2/(2m_0)$.

[30] J. M. Pitarke and A. G. Eguiluz, Phys. Rev. B **63**, 045116 (2001).

[31] F. K. Schulte, Surf. Sci. **55**, 427 (1976).

[32] N. W. Ashcroft and N. D. Mermin, *Solid State Physics* (Holt, Rinehart and Winston, Cornell University, 1976).

[33] For the homogeneous three-dimensional (3D) electron gas, one has an analytical expression for the HF eigenvalues, and then it is easy to show that they exhibit a divergent slope at the Fermi level, and that the HF DOS is exactly zero when evaluated at the Fermi level. The same is true for our 3D inhomogeneous situation, but due to the numerical accuracy, the infinite slope and zero DOS are only approximately realized.

[34] The discussion in this paragraph has been focused on a particular slab ($r_s = 6$). However, it qualitatively applies equally well to slabs of other sizes at other densities. Quantitatively, some differences emerge when, for example, the slab density changes. Thus, for example, for the same slab but with $r_s = 2$ (higher density, left panel in Fig. 1), the anomalous features of the HF band structure become less marked. In particular, the HF bandwidth is just a factor of about two greater than the x-LDA and x-OEP bandwidths. This is of course in line with the well-known fact that in the high-density limit ($r_s \to 0$), exchange (and correlation) effects become relatively less important than single-particle effects (the kinetic energy here).

[35] Note that the dimensions of Eqs. (2.1) and (2.3) are (length)$^{-3}$, which corresponds to our 3D system. For the particular case of the slab geometry, however, this 3D number density only depends on one spatial coordinate (z).

[36] N. D. Lang and W. Kohn, Phys. Rev. B **1**, 4555 (1970).

[37] In the DFT common language, the electrostatic potential is the sum of the Hartree and external potentials, with the first being generated by $\rho(z)$, and the second being generated by $\rho_+(z)$.

[38] L. Kleinman, Phys. Rev. B **49**, 14197 (1994).

[39] W. Kohn and A. E. Mattsson, Phys. Rev. Lett. **81**, 3487 (1998). They refer to the negative of this magnitude as the "inverse radius of the exchange hole," and use the symbol $R_x^{-1}(\mathbf{r})$.

[40] C. M. Horowitz, C. R. Proetto, and S. Rigamonti, Phys. Rev. Lett. **97**, 026802 (2006).

[41] S. Kummel and J. P. Perdew, Phys. Rev. B **68**, 035103 (2003).

[42] Note that this strict equivalence is only valid in this specific case (shifts being identically zero). As soon as the shifts are allowed to be different from zero, self-consistently calculated $V_{x,1}(z)$ and $V_x^{\mathrm{KLI}}(z)$ will not be equal due to the presence of $V_{x,2}(z)$.

[43] J. Bardeen, Phys. Rev. **49**, 653 (1936).

[44] G. F. Giuliani and G. Vignale, *Quantum Theory of the Electron Liquid* (Cambridge University Press, Cambridge, 2005).

[45] $E_{\mathrm{bulk}}(L,r_s)$ is the ground-state energy of a *uniform* slab of electron gas of size L and density ρ_0. Accordingly, we have taken $E_{\mathrm{bulk},K}(L,r_s) = (3\pi^2\rho_0)^{5/3} LS/(10\pi^2)$ H, $E_{\mathrm{bulk},el}(L,r_s) = 0$, and $E_{\mathrm{bulk},x}(L,r_s) = -3(3\pi^2)^{1/3}(\rho_0)^{4/3} LS/(4\pi)$ H.

[46] N. D. Lang, in *Solid State Physics*, edited by H. Eirenreich, F. Steitz, and D. Turnball (Academic, New York, 1973), Vol. 28, p. 225.

[47] T. Koopmans, Physica **1**, 104 (1933).

[48] J. P. Perdew and M. R. Norman, Phys. Rev. B **26**, 5445 (1982).

[49] E. Engel and R. M. Dreizler, J. Comput. Chem. **20**, 31 (1999).

[50] F. K. Schulte, J. Phys. C **7**, L370 (1974); E. E. Mola and J. L. Vicente, J. Chem. Phys. **84**, 2876 (1986); J. L. Vicente *et al.*, Physica Status Solidi B **155**, K93 (1989). Quite generally, these oscillations of slab properties (the work function in this case) as a function of the slab thickness are termed quantum-size effects (QSE). Using this language, the small oscillations of the HF and x-LDA work functions may be termed as weak QSE, while the large discontinuities of the x-OEP work function may be characterized as strong QSE.

[51] C. M. Horowitz, C. R. Proetto, and J. M. Pitarke, Phys. Rev. B **81**, 121106(R) (2010).

[52] N. C. Handy, M. T. Marron, and H. J. Silverstone, Phys. Rev. **180**, 45 (1969).